Thermal properties, texture, second-order stress, and magnetic susceptibility of the Bi1.8Pb0.3Sr2Ca2Cu3.3Ox

ARTICLE *in* JOURNAL OF THERMAL ANALYSIS AND CALORIMETRY · OCTOBER 2014

Impact Factor: 2.04 · DOI: 10.1007/s10973-014-4010-1

3 AUTHORS, INCLUDING:

Ana Harabor

University of Craiova

29 PUBLICATIONS **116** CITATIONS

SEE PROFILE

Petre Rotaru

University of Craiova

70 PUBLICATIONS **394** CITATIONS

SEE PROFILE

J Therm Anal Calorim (2014) 118:227–234
DOI 10.1007/s10973-014-4010-1

Thermal properties, texture, second-order stress, and magnetic susceptibility of the $Bi_{1.8}Pb_{0.3}Sr_2Ca_2Cu_{3.3}O_x$

Ana Harabor · P. Rotaru · N. A. Harabor

Received: 11 February 2014 / Accepted: 3 July 2014 / Published online: 1 August 2014

Abstract Mono-phase high critical temperature (Bi,Pb)-2223 superconductor from the off-stoichiometric $Bi_{1.8}Pb_{0.3}Sr_2Ca_2Cu_{3.3}O_x$ belonging to the tetragonal system, has been obtained. We studied the crystalline structure, the stress of second order, and the texture of the surface pellet, in the framework of XRD diffractometry. Results of the thermal measurements made in the nitrogen, with a heating rate of 10 K min^{-1}, from room temperature (RT) to 1273.15 K, show a slow mass decrease of 1.25 % from RT to 1003.15 K probably due to the elimination of water, oxygen, and of the other gases accumulated on the crystallite surface through chemical adsorption. Two endothermic processes were evidenced on DSC, and DTG curves: the first in the range of 1135.15–1193.15 K (melting and slow decomposition), and another after 1217.45 K (decomposition). The contribution of crystal lattice to the estimated specific heat capacity was in conformity with the Einstein model, giving for the Einstein temperature a value of 1297.5 K. In conformity with the Müller critical state model, we found linear dependences for intragrain critical transition temperature, T_g, and intergrain coupling temperature, T_p, versus the amplitude of the external AC magnetic fields. There was evidenced that intergrain critical currents are five orders smaller than the intragrain critical currents.

A. Harabor · P. Rotaru
Department of Physics, University of Craiova, 13 A.I. Cuza Street, 200585 Craiova, Romania

N. A. Harabor (✉)
Department of Physics, Faculty of Applied Sciences, Politehnica University of Bucharest, 313 Splaiul Independenţei blvd, 060042 Bucharest, Romania
e-mail: adrian.harabor@yahoo.com

Keywords (Bi,Pb)-2223 · XRD · Thermal properties · AC magnetic susceptibility

Introduction

Soon after the discovery of the Bi–Sr–Ca–Cu–O system by Maeda et al. [1], the researchers hardly worked to synthesize and stabilise the high critical temperature (T_c) superconductive, Bi-2223 single phase, due to the very narrow range of temperature for sintering this phase [1–11]. For the Bi–Sr–Ca–Cu–O system were obtained at least three different superconducting phases: $Bi_2Sr_2CuO_6$ (2201 phase with T_c of 10–20 K), $Bi_2Sr_2CaCu_2O_8$ (2212 phase with T_c of 80 K), and $Bi_2Sr_2Ca_2Cu_3O_{10}$ (2223 phase with T_c of 110 K).

It was descovered that the partial substitution of Bi by Pb helps in the stabilization [2, 3] of the high-T_c phase. Using the well-established techniques of glass technology such as the melt quenching approach one can fabricate dense ceramic superconductors, without pores, into desired shapes (wires, tapes, fibers, etc.), promising high critical current densities.

We reported in earlier papers [4, 10, 11] on the synthesis of a mono-phase high T_c (Bi,Pb)-2223 superconductor from the off-stoichiometric $Bi_{1.8}Pb_{0.3}Sr_2Cu_{3.3}O_x$ (by adding PbO and excess of Cu) in a long time sintering (600 h), the pellets being pressed at high isostatic pressure of 170 MPa before sintering in flowing nitrogen atmosphere. In this paper, we report on the results of XRD analysis giving information about the presence of the second-order stress [12], as well as, the evidence of the grains partial orientation on the pellet surface (the pressure axis being perpendicular on it). Thermal investigations of this mono-phase (Bi,Pb)-2223 sample (prepared by us) were

performed for the first time, and the results of the heat capacity calculation will be discussed. The alternative current (AC) susceptibility measurements are contact-less and completely non-destructive. Two peaks can be seen on the curve representing the temperature dependence of the imaginary part, χ'', of the complex AC susceptibility: the first appears at a temperature T_g close to T_c, and belongs to intragranular losses (motion of intragrain Abrikosov vortices); the second peak is located at a temperature T_p lower than T_c and corresponds to the intergranular loss due to the motion of Josephson intergranular vortices [7, 13]. From magnetic AC susceptibility data, we calculated intragrain critical transition temperature (T_g), and intergranular coupling temperature (T_p), corresponding to the largest contribution to the energy loss versus AC amplitude of the external magnetic field.

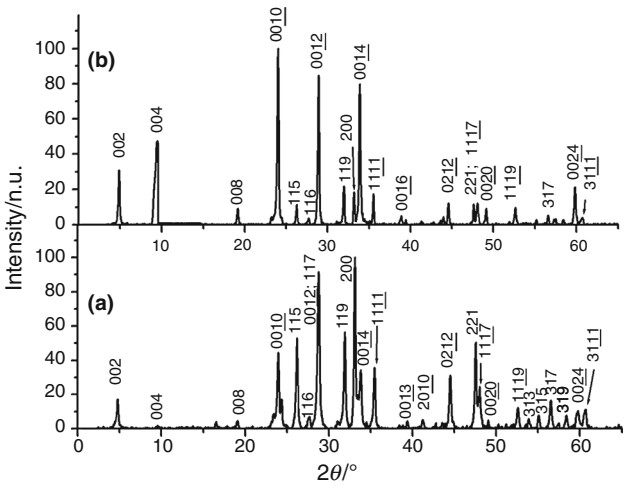

Fig. 1 XRD-$K_{\alpha 1}$ patterns of (Bi,Pb)-2223 powder in 0–70°. 2θ range: **a** powder sample; **b** pellet sample

Experimental

Sample preparation

The (Bi,Pb)-2223 mono-phase pellet was prepared by the solid-state reaction method [4, 5, 10, 11]. We have chosen an off-stoichiometric composition $Bi_{1.8}Pb_{0.3}Sr_2Ca_2Cu_{3.3}O_x$ with excess of Pb, Bi, and Cu. The starting materials were high purity (99.99 %) powders of Bi_2O_3, PbO, $CaCO_3$, $SrCO_3$, and CuO from Merck KGaA Company. The mixed powder was calcinated at 1073.15 K for 38 h. The resulting materials were ground, then isostatically pressed at 170 MPa into pellets, sintered at 1103.15 K in flowing N_2 gas for 6 days, and finally air quenched. The sintering was repeated three times in flowing N_2 gas: for 7 days at 1119.15 K, 5 days at 1120.15 K, and 7 days at 1117.15 K, respectively; the second and the third sintering treatments were followed by air quenching, but after the fourth sintering treatment the samples were furnace cooled to room temperature in flowing N_2 atmosphere. The sample pressed at 170 MPa has a density of 4.18 g cm^{-3}.

Methods and techniques

XRD measurements were performed on powder samples, with a Shimadzu XRD-6000 X-ray diffractometer, equipped with a vertical goniometer and a scintillation detector. The functioning parameters of the X-ray tube (40-Cu type) were set at a voltage of 40 kV and a current of 30 mA. A continuous scan measurement has been chosen as operation mode in geometry ($\theta/2\theta$), setting a scan 2θ rate of 1° min^{-1} and a scan 2θ range from 2 to 80°. Divergence slit was of 1.0000°, scattering slit was of 1.0000°, and receiving slit of 0.1500 mm.

Thermal analysis measurements (TG, DTG, and DSC) of (Bi,Pb)-2223 compound were carried out in dynamic air atmosphere (150 cm^3 min^{-1}). A horizontal "Diamond" differential/thermogravimetric analyzer from PerkinElmer Instruments was used during the measurements. The thermogravimetric and enthalpic calculations were performed with the specialized software Pyris.

The AC susceptibility versus temperature measurements at fixed AC magnetic field amplitudes from 0.4 to 800 A m^{-1}, were performed with a Lake Shore Model 7000 AC Susceptometer at a frequency of 777.7 Hz. Bar specimens with the dimensions of 2.59, 2.13, 4.29 mm were cut from the sintered sample and introduced into the secondary coil with the longest dimension parallel to the field. The sample was cooled down in zero fields and then warmed up at a constant rate of 0.5 K min^{-1}. The data acquisition was made by a computer after stabilizing the temperature.

Results and discussion

Crystalline structure of (Bi,Pb)-2223

As seen from Fig. 1, the Bragg diffraction patterns, obtained for $\lambda = 1.54045$ Å (Cu $K_{\alpha 1}$, X-ray radiation), indicate a mono-phase tetragonal crystalline structure for our (Bi,Pb)-2223 samples (powder and pellet) prepared as presented above.

For indexing diffraction patterns, we were guided by a similar tetragonal structure given in the card c42-0415 [3] taken from 2001 JCPDS-international Centre for Diffraction Data (PCPDFWIN v.2.2).

By X-ray diffraction, performed with a Shimadzu XRD 6000 Diffractometer using a Cu K_α source, we indexed the unit cell of (Bi,Pb)-2223 powder compound, as belonging to the tetragonal system, verifying the well-known Equation [12, 14].

$$\frac{1}{d_{hkl}^2} = \frac{h^2 + k^2}{a^2} + \frac{l^2}{c^2}, \quad (1)$$

where d_{hkl} are the interplane distances, h, k, l—the Miller indexes for diffraction planes, and $a = b$, c are the lattice parameters of the unit cell.

Table 1 shows main XRD peaks of (Bi,Pb)-2223-powder (relative intensities, d_{hkl}-inter-plane distances, 2θ-diffraction angles, and hkl-Miller indexes for diffraction planes).

The experimental lattice parameters were calculated using the least square refinement from a Shimadzu adequate program, obtaining the following cell parameters: $a = b$ = 5.4049 Å and c = 37.1134 Å. This proves a structural organization degree at long range. There are some approximation methods to define the breadth β in the Scherrer formula to calculate the average crystallite sizes [14]. In the assumption of ellipsoidal particles [15–18], it is found that the Jones more purely empirical approach will provide the best means for making allowance for the dimensions of the samples. In this last case using the integral breadths (β_i), when $k = 1.333$, we obtained for (Bi,Pb)-2223 particle dimensions a mean value of about 42.98 nm.

Table 1 Main XRD peaks of (Bi,Pb)-2222 powder

Relative intensity	d_{hkl}/Å	2θ/°	hkl
100	2.0185	33.298	200
91	3.9623	28.114	00$\underline{12}$
56	2.0076	31.279	119
53	3.9692	26.133	115
50	1.908	47.66	221
44	3.1134	23.617	00$\underline{10}$
36	2.2905	35.659	1$\underline{11}$1
34	2.5169	33.75	00$\underline{14}$
31	2.3365	44.58	02$\underline{12}$
25	1.9200	48.05	11$\underline{17}$
20	2.7361	33.9	202
17	18.503	4.856	002
16	1.2665	56.298	317
12	1.3825	52.102	11$\underline{19}$
10	1.4649	59.83	00$\underline{24}$
9	3.8018	23.38	111
8	1.5794	58.38	319
7	3.2513	27.43	116
6	1.6600	55.02	315
5	4.6441	19.095	008
5	2.1864	41.2575	20$\underline{10}$
5	1.8543	49.0916	00$\underline{20}$
5	1.6931	55.16	313

It has been shown [19–23] that the role of the lead is to accelerate the growth of the 2223 phase by enhancing diffusion of calcium and copper during insertion of an extra layer of Ca–O and Cu–O into the unit cell of 2212: the 2212 phase is always formed first [19] because 2223 phase needs a higher free energy due to a longer c-axis of its unit cell. Pb atoms are known to partially substitute [20, 21] into the Bi–O layers of the crystal structure of the 110 K phase as it was evidenced by high resolution analytical electron microscopy [23]. The lead is easily incorporated into the structure probably because Bi (in the +3 oxidation state) and Pb (in the +2 state) have similar outer electronic configuration [23]. The substitution of the bigger Pb^{2+} cation (ionic radius = 1.20 Å) for Bi^{3+} (ionic radius = 0.96 Å) probably leads to the distortion of the crystal lattice [20–23].

By comparing XRD spectrum performed on the pellet surface (Fig. 1b) with those obtained for the (Bi,Pb)-2223 powder (Fig. 1a), we observed partial orientation of the grains with the c-axis perpendicular to the specimen surface, e.g., parallel to the pressure axis. In this context, from Fig. 1, where are given relative intensities of diffraction picks over 2θ angle, for powder and pellet, respectively, it is evident that in the case of pellet surface it occurs an increase of the intensity for the picks (002), (004), (008), (00$\underline{10}$), (0012), (00$\underline{14}$), (00$\underline{20}$), and (00$\underline{24}$) while the intensities of the other picks ((200), (119), (115), (221), (11$\underline{11}$), (02$\underline{12}$), (11$\underline{17}$), (202), (317), (11$\underline{19}$), (111), (319), (116), (315), (20$\underline{10}$), and (313)) are falling down.

The partial orientation of the grains is also evidenced by SEM investigation of the pellet surface, as shown elsewhere [10].

In Fig. 2a, b are represented the following two dependences for integral breadths (β_i) versus θ angle:

$$\text{(a)} \quad \beta_i = f(tg\theta), \quad (2)$$

$$\text{(b)} \quad \beta_i = f\left(\frac{\lambda}{\cos\theta}\right). \quad (3)$$

In the hypothesis of a supplementary broadening of the picks produced by the modification of the crystallite dimensions, it should be found a linear dependence of the integral breadth β_i versus ($\lambda/\cos\theta$) [12]. The experimental data represented in Fig. 2b do not exhibit a clear dependence of this type. Instead, from Fig. 2a, it is verified an evident linear dependence for our data giving β_i versus ($tg\theta$), of the type (4):

$$\beta_i = 0.357 + 0.429 \cdot tg\theta. \quad (4)$$

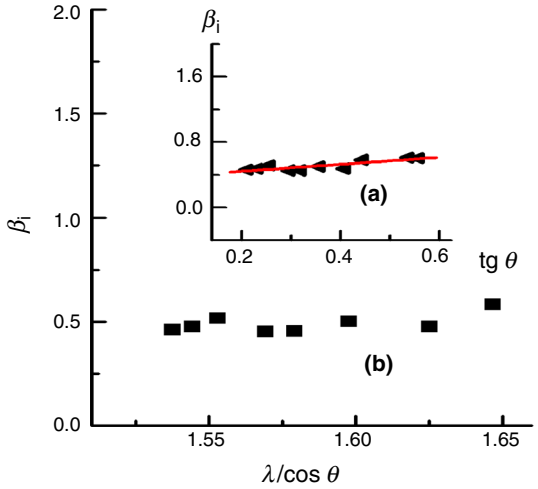

Fig. 2 Evidence of second-order stress in (Bi,Pb)-2223 powder

The Eq. (4) characterizes the presence of the internal second-order stress [12].

In Fig. 3, the relative deformation ($\Delta d/d$) of the interplanar distances caused by second-order stress was calculated with the formula (5) [12, 14]:

$$\frac{\Delta d}{d} = \frac{\beta_i}{4tg\theta}. \quad (5)$$

For high values of Miller indexes, ($\Delta d/d$) versus d_{hkl}-interplanar distances verify a linear dependence of the type (6):

$$\frac{\Delta d}{d} = 0.051 + 1.32 d_{hkl}. \quad (6)$$

The value of the second-order stress (σ_{II}) can be calculated with the relation (7), expressing the Hooke law, if the Young constant, E, is known [12]:

$$\sigma_{II} = E\frac{\Delta d}{d}. \quad (7)$$

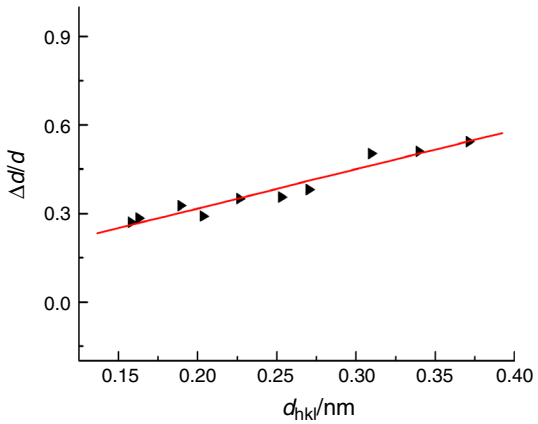

Fig. 3 Relative elongation over interplanar distances d_{hkl}

Thermal characteristics of (Bi,Pb)-2223

Thermal analysis is frequently used to determine the thermal stability and phase transformations of organic and inorganic materials [24–38].

The thermal measurements were made on the (Bi,Pb)-2223 specimen, after the last annealing. An initial mass of 21.51 mg was heated in nitrogen, with a heating rate of 10 K min^{-1}, from (RT) to 1273.15 K.

In Fig. 4 are given TG, DTG, and DSC curves. It is seen from TG that in the temperature range from RT to 1,003.15 K, a mass loss of 0.27 mg (1.25 %) takes place, due to the elimination of the water, oxygen, and of the other gases accumulated on the crystallite surface through physical and chemical adsorption [39].

We observed a relative good stability in the ranges 660.15–870.15 and 1,003.15–1,135.15 K. A strong endothermic effect of melting together with a small decomposition probably due to oxygen loss (as shown by DSC and DTG) takes place between 1,135.15 and 1,193.15 K, with a mass loss of 0.24 mg (1.11 %). The maximum temperature of this endothermic effect was of 1,162.65 K. The enthalpy calculation (shown in Fig. 5) of the melting and decomposition process is of 137.9 J g^{-1}. Another minor endothermic process of decomposition takes place beginning with the temperature of 1,217.45 K giving until 1,265.15 K a mass loss of 0.08 mg (0.37 %).

Specific heat capacity was calculated using the formula (8) [12, 16]:

$$c_p = \frac{1}{m}\frac{\delta Q}{dT} = \frac{1}{m}\frac{(\delta Q/d\tau)}{(dT/d\tau)}. \quad (8)$$

In expression (8), ($dQ/d\tau$) is the heat flux given by the DSC curve, m is the sample mass, and ($dT/d\tau$) = 10 K min^{-1} is the heating rate of the sample.

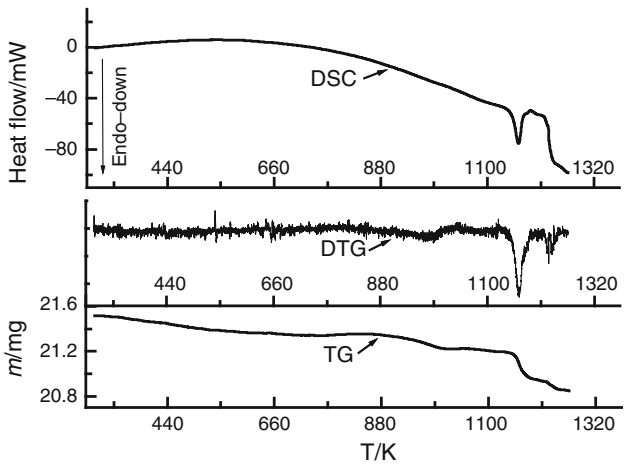

Fig. 4 TG and DSC diagrams obtained for a heating rate of 10 K min^{-1} in the range from room temperature to 1273 K for the (Bi,Pb)-2223 sample

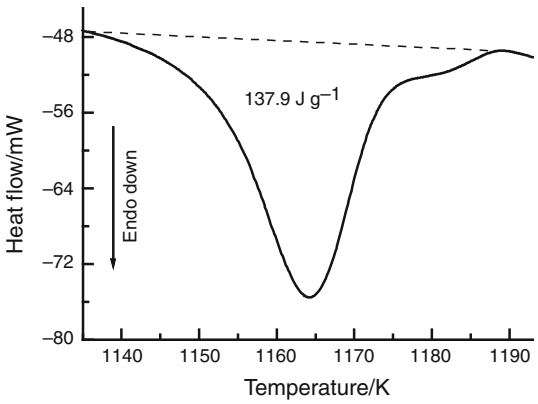

Fig. 5 The enthalpy calculation in the endothermic process (endo down) from 1,135.15 to 1,193.15 K

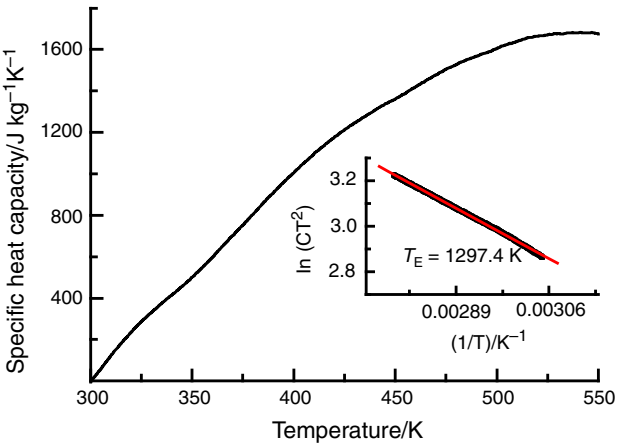

Fig. 6 Specific heat capacity over temperature for (Bi,Pb)-2223 powder in temperature ranges from 300 to 550 K. For low temperatures range (328.07–360.25 K), in the *inset* of figure is given the experimental plots and the regression line in conformity with the Einstein model

From Fig. 6 is observed the metalic behavior of the compound from 300 to 543 K, having six linear dependences (Eqs. 9–14) for the specific heat capacity (c_p) over temperature, corresponding to different temperature ranges:

$$c_p = (-3442.4_{\text{err:9}} + 11.491_{\text{err:0.024}}T)\ \text{J kg}^{-1}\ \text{K}^{-1} \quad \text{in the range } 300-325\ \text{K}, \tag{9}$$

$$c_p = (-2991.9_{\text{err:3}} + 9.988_{\text{err:0.084}}T)\ \text{J kg}^{-1}\text{K}^{-1} \quad \text{in the range } 341-415\ \text{K}, \tag{10}$$

$$c_p = (-1666.8_{\text{err:7.6}} + 6.770_{\text{err:0.017}}T)\ \text{J kg}^{-1}\text{K}^{-1} \quad \text{in the range } 415-438\ \text{K}, \tag{11}$$

$$c_p = (-1158.9_{\text{err:3.2}} + 5.606_{\text{err:0.069}}T)\ \text{J kg}^{-1}\text{K}^{-1} \quad \text{in the range } 438-482\ \text{K}, \tag{12}$$

$$c_p = (-71.9_{\text{err:7.8}} + 3.350_{\text{err:0.015}}T)\ \text{J kg}^{-1}\text{K}^{-1} \quad \text{in the range } 482-523\ \text{K} \tag{13}$$

$$c_p = (+1262.1_{\text{err:3}} + 0.778_{\text{err:0.015}}T)\ \text{J kg}^{-1}\text{K}^{-1} \quad \text{in the range } 523-543\ \text{K}. \tag{14}$$

The contribution of crystal lattice to the specific heat capacity could be studied in the framework of the Einstein model. In conformity with the Einstein model [12, 16], where the three *N*-independent oscillators are considered to describe a system of *N* atoms, we have calculated the Einstein temperature (T_E) from the expression (15) for the heat capacity (C):

$$C = 3R\left(\frac{T_E}{T}\right)^2 e^{-\frac{T_E}{T}}. \tag{15}$$

In our case, the Einstein model seems to be quite well verified for low temperatures (from 328.07 to 360.25 K) as we found a linear fit (see the inset of Fig. 6) describing the curve $\ln(CT^2) = f(1/T)$, as given in Eq. (16):

$$\ln\left(CT^2\right) = 6.8276_{\text{err:0.0048}} - 1297.4_{\text{err:1.6}}\left(\frac{1}{T}\right). \tag{16}$$

This permited us to calculate the Einstein temperature (T_E) as having a value of $T_E = (1297.4 \pm 1.6)$ K.

We have to remark that on DSC curve we did not detect any glass transition (endotherm efect) at 383 °C (656.15 K) or crystallization process (exotherm) at 446 °C (716.15 K) that are characteristic to the phase $Bi_2Sr_2CuO_6$ (2201 phase) as shown in [3]: this proved the absence of (2201) phase in our sample. Also, we did not observe any other small peaks at 720 °C (993.15 K) and 753 °C (1026.15 K) as in [3] being responsible for the formation of various crystalline phases (as 2212 phase or others). In conclusion, thermal analysis validate the high purity in 2223 phase of the prepared sample.

Temperature dependence of AC susceptibility for (Bi,Pb)-2223

In order to decrease the demagnetisation factor D, the rectangular samples were oriented with the longest size parallel to the AC magnetic field.

In [4, 10, 21] was shown that the diamagnetic signal is strongly influenced by the sintering time, due to the continuous increase of the amount of the 2223 phase, while the 2212 phase is diminished.

In Fig 7a are represented the two curves (real, χ', and imaginary, χ'') representing the susceptibility data versus temperature, performed for a (Bi,Pb)-2223 pellet pressed at 170 MPa, at an external field of 0.4 A m^{-1}. In this case, we found a critical temperature (T_c) of 108.23 K as being the value for the diamagnetic onset of the superconductive

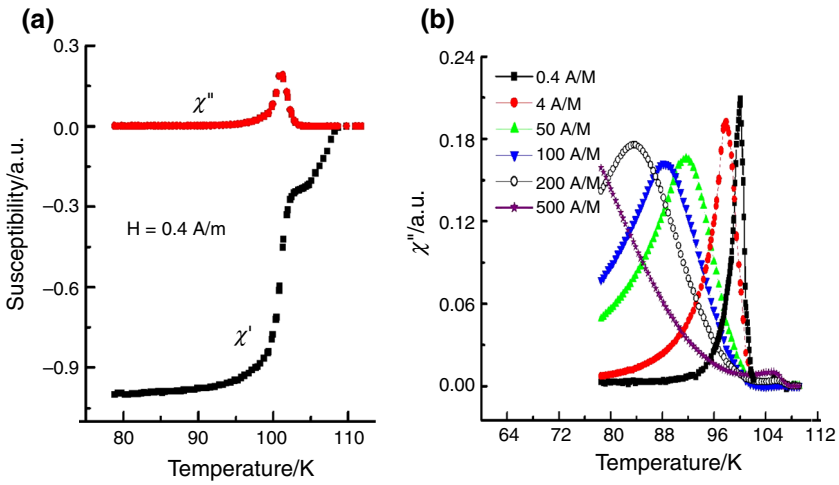

Fig. 7 **a** AC susceptibility (real and imaginary parts) over temperature for an external field of 0.4 A m^{-1}; **b** The imaginary part of the AC susceptibility for six different external AC magnetic fields

transition inside the grains. In Fig. 7b is given the imaginary part of the AC susceptibilities for the monophasic polycrystalline (Bi,Pb)-2223 obtained at a frequency of 777.7 Hz and at different external AC magnetic fields: 0.4, 4, 50, 100, 200, 500, and 800 A m^{-1}. Two drops are observed on real part of susceptibility (χ'): the first is related to the change of χ' from zero to negative, that is taking place at a temperature named intragrain critical transition temperature (T_g). The maximum hysteresis loss inside the grain is recorded at T_g and is due to the motion of intragranular (Abrikosov) vortices [7]. The second drop is recorded, both from real χ' as well as from imaginary part, and it is related to the intergranular coupling being recorded at a temperature, T_p. At a low magnetic field of 0.4 A m^{-1}, only the intergranular (Josephson) peak is visible, as it gives the largest contribution to the energy loss [4, 5, 7, 9].

We found linear dependences (solid lines given in Fig. 8) for the experimental T_g and T_p data as a function of AC magnetic field amplitude, as those given in Eqs. (17, 18):

$$T_g = \left(107.08 - 5.3 \times 10^{-3} H_{AC}\right) \text{ K}, \tag{17}$$

$$T_p = \left(95.59 - 5.69 \times 10^{-2} H_{AC}\right) \text{ K}. \tag{18}$$

The Eqs. (17, 18) should be interpreted within the framework of Müller critical state model [4, 7, 9, 12, 40, 41] if we compare them with the similar theoretical linear relations (19, 20):

$$T_g = T_C \left(1 - H_{AC} \sqrt{\frac{\mu_0 \cdot}{4 \cdot D_g \cdot \gamma_g^{0K}}}\right), \tag{19}$$

$$T_p = T_{p0} \left(1 - H_{AC} \sqrt{\frac{\mu_0 \cdot \mu_{eff}^{0\,K}}{2 \cdot d \cdot \gamma_p^{0\,K}}}\right). \tag{20}$$

Here $\gamma_g^{0\,K}$ and $\gamma_p^{0\,K}$ are the pinning force densities independent of magnetic flux for intra and intergranular vortices; μ_0 is the magnetic permeability in vacuum, $\mu_{eff}^{0\,K}$ is the

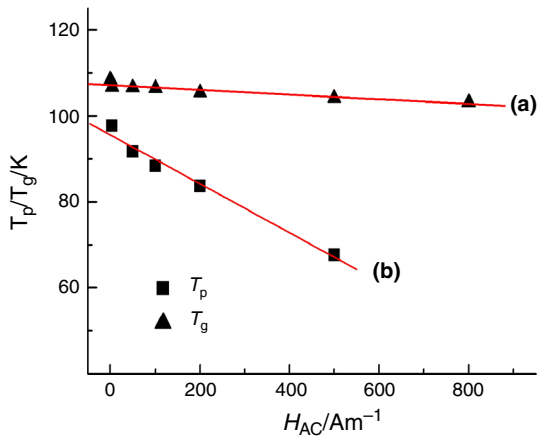

Fig. 8 **a** Intragranular χ''-peak temperature, T_g, versus AC field amplitude, H_{AC}; **b** intergranular peak temperature, T_p, versus H_{AC}

effective magnetic permeability at $T = 0$ K, approximated by the normal volume fraction of sample, D_g is the grain diameter of superconducting cylinders, d is the thickness of the sample.

Taking $D_g = 30$ μm, $d = 1$ mm, $\mu_{eff}^{0\,K} = 0.2$, we obtain $\gamma_g^{0\,K} = 11252\ \gamma_p^{0\,K}$. This provides that intergrain current density, J_{ci} is very small compared with the intragrain density J_{cg}.

The intergrains critical current densities (J_{ci}) were estimated in the framework of Bean critical state model. The dependence of J_{ci} over temperature (Fig. 9) exhibits in the temperature range of 93.6–99.4 K a polynomial fit of the form [4, 7, 9, 12, 21], given in Eq. (21):

$$J_{ci} = J_{ci}(0) \left(1 - \frac{T}{T_{p0}}\right)^2. \tag{21}$$

We obtained $J_{ci}(0) = 227.2$ A cm^{-2} and $T_{p0} = 98.8$ K, indicating that the intergrain junctions are of the superconductor-normal-superconductor (SNS) type. From

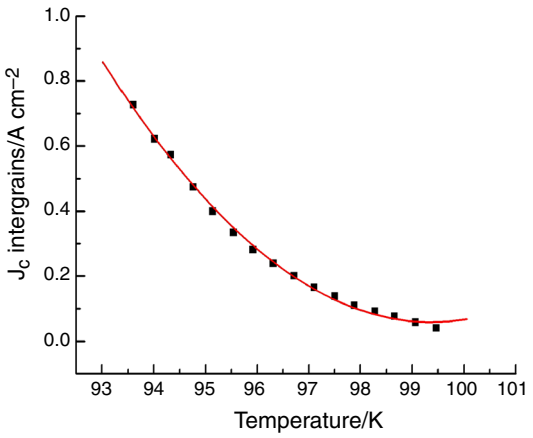

Fig. 9 The intergrains critical current density calculated at $H_{AC} = 0.4$ A m^{-1}

previous considerations, it results an estimation of the intragrain current at 0 K of about $J_{cg} \cong 2.556454 \times 10^7$ A cm^{-2}.

Conclusions

Using XRD analysis, the main diffraction maxima of the (Bi,Pb)-2223 powder have been identified as belonging to a tetragonal crystallization system, having the following lattice parameters: $a = b = 5.4049$ Å and $c = 37.1134$ Å. We obtained for (Bi,Pb)-2223 particle dimensions a mean value of about 42.98 nm. It has been determined through XRD measurements, partial alignment of crystallites on the sample surface, as well as, second-order stress. As shown by DSC, and DTG, a strong endothermic effect of melting & small decomposition is taking place in the range of 1135.15–1193.15 K, with a mass loss of 1.11 %. The maximum temperature of the peak, describing the endothermic effect was of 1162.65 K. A second small endothermic process of decomposition takes place beginning with the temperature of 1217.45 K giving another loss of about 0.37 % until 1265.15 K. The metalic behavior of the compound in the range from 300 to 543 K, was detected from the curve of specific heat capacity over temperature, having six linear dependences with different rates for different temperature ranges. Applying Einstein model, in the range (328.07–360.25 K), we calculated the Einstein temperature as being of $T_E = (1297.4 \pm 1.6)$ K. We hope that in a next paper, we will perform more investigations on the desorption of the adsorbed gases and vapors, as well as, on determination of oxygen content in the sample, using combined techniques TG-MS [42]. A critical temperature (T_c) of 108.23 K for superconductive transition was determined from susceptibility measurements. Linear dependences, in conformity with the Müller critical state model, have been found for the experimental intragrain peak temperature, T_g, and intergrain temperature, T_p, respectively, versus AC magnetic field amplitude. The intergrain critical current density was about five orders lower than the intragrain one.

Acknowledgements We thank to professor R Deltour from ULB Bruxelles for giving access to the facilities from his laboratory. Thank GOD for this.

References

1. Maeda H, Tanaka Y, Fukutomi M, Asano T. A new high-T_c oxide superconductor without a rare earth element. Jpn J Appl Phys. 1988;27:209–10.
2. Komatsu T, Sato R, Hirose C, Matusita K, Yamashita T. Preparation of high-T, superconducting Bi–Pb–Sr–Ca–Cu–O ceramics by the melt quenching method. Jpn J Appl Phys. 1988;27:2293–5.
3. Bansal NP, Farrell DE. Glass-derived superconducting ceramics with zero resistance at 107 K in the $Bi_{1.5}Pb_{0.5}Sr_2Ca_2Cu_3O_x$ system. Appl Phys Lett. 1989;55:1572–4.
4. Harabor A, Deltour R, Ye M, Schroeder J, Hancotte H, Moortgat G, Deletter M. Weak-link behavior for 2223 polycrystalline (Bi,Pb)–Sr–Ca–Cu–O single phase. Superlattice Microstruct. 1997;21:229–33.
5. Harabor A, Pop AV, Deltour R, Schroeder J, Ciurchea D, Ilonca Gh. Intergranular critical currents and excess conductivity in the Fe-substituted Bi-2223 high T_c superconductor. J Low Temp Phys. 1996;105:1053–9.
6. Pop AV, Deltour R, Ciurchea D, Harabor A, Ilonca Gh, Coldea S. Activation energies in the vortex liquid state of bulk $(Bi_{1.6}Pb_{0.4})(Sr_{1.8}Ba_{0.2})Ca_2Cu_3O_y$ superconductor. Mod Phys Lett B. 1996;10:1453–60.
7. Pop AV, Deltour R, Harabor A, Ciurchea D, Ilonca Gh. AC susceptibility study of the inter- and intragranular properties in (Bi,Pb): 2223 superconductor. Int J Mod Phys B. 1997;11:3461–7.
8. Pop AV, Deltour R, Harabor A, Ciurchea D, Ilonca Gh, Pop V, Todica M. Effect of Fe substitution for Cu in the mixed state of (Bi,Pb): 2223 superconductor. Supercond Sci Tech. 1997;10:843–6.
9. Pop AV, Ciurchea D, Ilonca Gh, Harabor A, Deltour R. Superconducting properties in bulk $(Bi_{1.6}Pb_{0.4})(Sr_{1.8}Ba_{0.2})12Cu_3O_y$ system. Phys C. 1997;282(287):2365–6.
10. Harabor A, Harabor NA. Pressure effect on optical conductivity for bulk (Bi,Pb)-2223 samples. J Optoelectron Adv Mater. 2006;8:1065–71.
11. Harabor A, Harabor NA, Deletter M. Short-wavelength fluctuation regime in paraconductivity of bulk monophase (Bi,Pb)-2223 superconductor system. J Optoelectron Adv Mater. 2006;8:1072–6.
12. Pop V, Chicinas I, Jumate N. Material physics. Experimental methods. Cluj-Napoca: Presa Universitara Clujeana House; 2001.
13. Gencer A, Nezir S, Altunbas M, Aydinuraz A. AC susceptibility study of BiPbSrCaCuO(2223) superconductors. Supercond Sci Technol. 1996;9:467–73.
14. Cullity B. Elements of X-ray diffraction. Reading: Addison-Wesley; 1978.
15. Patterson AI. The Scherrer formula for X-ray particle size determination. Phys Rev B. 1939;56:978–82.
16. Harabor A, Rotaru P, Harabor NA. Thermal and spectral behavior of (Y, Eu)VO_4 powder. J Therm Anal Calorim. 2013;111:1211–9.

17. Pascu CI, Gingu O, Rotaru P, Vida-Simiti I, Harabor A, Nicoleta Lupu N. Bulk titanium for structural and biomedical applications obtaining by spark plasma sintering (SPS) from titanium hydride powder. J Therm Anal Calorim. 2013;113:849–57.
18. Moanţă A, Ionescu C, Rotaru P, Socaciu M, Hărăbor A. Structural characterization, thermal investigation, and liquid crystalline behavior of 4-[(4-chlorobenzyl)oxy]-3,4′-dichloroazobenzene. J Therm Anal Calorim. 2010;102:1079–86.
19. Shi D, Boley MS, Chen JG, Xu M, Vandervoort K, Liao YX, Zangvi A, Akujieze J, Segre C. Origin of enhanced growth of the 110 K superconducting phase by Pb doping in the Bi–Sr–Ca–Cu–O system. Appl Phys Lett. 1989;55:699–701.
20. Takano M, Takada J, Oda K, Kitaguchi H, Miura Y, Ikeda Y, Tomii Y, High-T Mazaki H. Phase promoted and stabilized in the (Bi,Pb)–Sr–Ca–Cu–O system. Jpn J Appl Phys. 1988;27:1041–3.
21. Harabor A. Experimental researches with HTSC superconductors. Craiova-Romania: Universitaria House; 2003.
22. Mizuno M, Endo H, Tsuchiya J, Kijima N, Sumiyama A, Oyuri Y. Superconductivity of $Bi_2SrCa_2Cu_3PbO$ ($x = 0.2$, 0.4,0.6). Jpn J Appl Phys. 1988;27:1325–7.
23. Nobumasa H, Arima T, Shimizu K, Otsuka Y, Murata Y, Kawai T. Observation of the high-T_c phase and determination of the Pb position in a Bi–Pb–Sr–Ca–Cu oxide superconductor. Jpn J Appl Phys. 1989;28:57–9.
24. Rotaru P, Scorei R, Hărăbor A, Dumitru MD. Thermal analysis of a calcium fructoborate sample. Thermochim Acta. 2010;506: 8–13.
25. Rotaru A. Thermal analysis and kinetic study of Petrosani bituminous coal from Romania in comparison with a sample of Ural bituminous coal. J Therm Anal Calorim. 2012;110:1283–91.
26. Samide A, Tutunaru B, Negrilă C, Dobriţescu A. Study of the corrosion products formed on carbon steel surface in hydrochloric acid solution. J Therm Anal Calorim. 2012;110:145–52.
27. Rotaru A, Moanta A, Sălăgeanu I, Budrugeac P, Segal E. Thermal decomposition kinetics of some aromatic azomonoethers. Part I. Decomposition of 4-[(4-chlorobenzyl)oxy]-4′-nitro-azobenzene. J Therm Anal Calorim. 2007;87:395–400.
28. Rotaru A, Kropidłowska A, Moanta A, Rotaru P. Thermal decomposition kinetics of some aromatic azomonoethers. Part II. Non-isothermal study of three liquid crystals in dynamic air atmosphere. J Therm Anal Calorim. 2008;92:233–8.
29. Rotaru A, Moanta A, Rotaru P, Segal E. Thermal decomposition kinetics of some aromatic azomonoethers. Part III. Non-isothermal study of 4-[(4-chlorobenzyl)oxy]-4′-chloro-azobenzene in dynamic air atmosphere. J Therm Anal Calorim. 2009;95:161–6.
30. Rotaru A, Moanta A, Popa G, Rotaru P, Segal E. Thermal decomposition kinetics of some aromatic azomonoethers. Part IV. Non-isothermal kinetics of 2-allyl-4-((4-(4-methylbenzyloxy) phenyl)diazenyl) phenol in dynamic air atmosphere. J Therm Anal Calorim. 2009;97:485–91.
31. Donato DI, Lazzara G, Milioto S. Thermogravimetric analysis. A tool to evaluate the ability of mixtures in consolidating waterlogged archaeological woods. J Therm Anal Calorim. 2010;101:1085–91.
32. Rotaru A, Goşa M, Rotaru P. Computational thermal and kinetic analysis. Software for non-isothermal kinetics by standard procedure. J Therm Anal Calorim. 2008;94:367–71.
33. Rotaru A, Goşa M. Computational thermal and kinetic analysis. Complete standard procedure to evaluate the kinetic triplet form non-isothermal data. J Therm Anal Calorim. 2009;97:421–6.
34. Badea M, Olar R, Marinescu D, Segal E, Rotaru A. Thermal stability of some new complexes bearing ligands with polymerizable groups. J Therm Anal Calorim. 2007;88:317–21.
35. Rotaru A, Bratulescu G, Rotaru P. Thermal analysis of azoic dyes: Part I. Non-isothermal decomposition kinetics of [4-(4-chlorobenzyloxy)-3-methylphenyl](*p*-tolyl)diazene in dynamic air atmosphere. Thermochim Acta. 2009;489:63–9.
36. Degeratu S, Rotaru P, Manolea Gh, Manolea HO, Rotaru A. Thermal characteristics of Ni–Ti SMA (shape memory alloy) actuators. J Therm Anal Calorim. 2009;97:695–700.
37. Gigante AC, Caires J, Gomes DJC, Lima LS, Treu-Filho O, Pivatto M, Ionashiro M. Spectroscopic study and thermal behavior of trivalent lanthanides and yttrium(III) chelates of EDTA using TG-DSC, FTIR, and TG-DSC coupled to FTIR. J Therm Anal Calorim. 2014;115:127–35.
38. Kannan T, Predeep P. Investigation into the superconducting threshold of $Bi_{1.6}Pb_{0.4}Sr_2Ca_{n\text{-}1}Cu_nO_{2n+4+d}$, $n = 2$, 2.5, 4 perovskites synthesized by glassy precursor route with thermal and Raman spectroscopic techniques. J Therm Anal Calorim. 2013;114:635–41.
39. Wolkenstein Th. Physico-chimie de la surface des semi-conducteurs. Moscou: Editions Mir; 1977.
40. Müller KH. AC susceptibility of high temperature superconductors in a critical state model. Phys C. 1989;159:717–26.
41. Müller KH, Farlane JC, Driver R. Josephson vortices and flux penetration in high temperature superconductors. Phys C. 1989;158:69–75.
42. Hauck J, Altenburg H, Bischof B, Denker S, Droste E, Ipta S, Plewa J. Variation of the oxygen content of lead-containing cuprates. Phys C. 1991;178:405–10.